

Effective Noise Reduction Filters for Precise Temperature Measurement Using Brillouin Distributed Optical Fiber Sensors

Jagonnath Biswas, Tanbin Ahmed, Sazzad M. S. Imran, and Abul Kalam Azad*

Department of Electrical and Electronic Engineering, University of Dhaka, Dhaka-1000, Bangladesh

**E-mail: azad@du.ac.bd*

Received on 14 September 2023, Accepted for Publication on 25 January 2024

ABSTRACT

This study explores the effectiveness of various noise reduction filters in accurately measuring temperature distributions over a 38.2 km single-mode fiber (SMF). Brillouin optical time-domain analysis (BOTDA) sensor is utilized to gather Brillouin gain spectra (BGSs), which are denoised using bilateral filter (BF), guided filter (GF), adaptive Wiener filter (AWF), non-local means filter (NLMF), average filter (AF) and disc filter (DF). The temperature distributions over the SMF are then determined by applying least-squares curve fitting (LSCF). The study assesses the efficacy of noise reduction filters considering signal-to-noise ratio (SNR), uncertainty in temperature measurement (UTM), experimental spatial resolution (ESR) and signal processing speed (SPS). Among six different filters, NLMF outperforms other filters which can provide SNR improvement of 10.22 dB for which the UTM can be improved by 58.93% without deteriorating the ESR of the sensor. The noise reduction using such filter can also provide 6.2% faster SPS. Therefore, NLMF can be considered as an effective noise reduction filter for the precise temperature measurement using BOTDA sensors.

Keywords: Optical fiber sensors, signal processing, noise reduction, least-squares curve fitting, temperature measurement.

1. Introduction

Distributed fiber-optic sensors provide unique capabilities for measuring different parameters in hazardous operating environments [1 – 3]. Such sensors are widely utilized for the monitoring of structural health [4], vibration [5], landslide [6] and temperature variations [7]. Brillouin optical time domain analysis (BOTDA) sensor is a specific type of fiber-optic sensor that excels at providing long range high temperature measurement with low uncertainty and excellent spatial resolution [7 – 10]. The BOTDA sensors with Brillouin gain setting involves launching pulsed pump and continuous probe waves to counter-propagate through the fiber. The high-power pump wave interacts with acoustic phonons in the fiber and generates the stimulation of Brillouin scattering [11]. The interaction involves transferring a fraction of pump energy to the probe wave, resulting in the probe wave being magnified. The magnified probe wave is recorded by scanning the pump-probe frequency difference step-by-step to obtain BOTDA-traces. These traces create Brillouin gain spectra (BGSs) over the SMF. The frequency at peak gain, also known as Brillouin frequency shift (BFS), in the local BGS exhibits a linear increase with temperature [7]. By measuring the BGSs at different fiber positions, we can resolve local BFSs, which in turn provide the temperature distribution along the fiber.

Relatively straightforward method of estimating the BFSs is the ‘maximum finding approach’ which identifies BFSs by detecting frequencies associated with peak gain of the BGSs [12]. However, the BGSs gathered from BOTDA experiment contain randomly distributed noises and experiences low

SNR due to relative intensity noise from laser source, amplified spontaneous emission (ASE) noise from EDFA, SBS-induced noise (SBSiN) due to pump-probe interaction, and shot and thermal noises from the detector [13, 14]. Such noise might elevate certain frequencies, leading to inaccurate BFSs. This limitation can be overcome by employing the least-squares curve fitting (LSCF) which involves fitting a suitable model function to the experimental data, allowing more accurate estimation of BFSs [7, 12]. However, low SNR at the termination of an extended SMF exacerbates the uncertainty in temperature measurement (UTM) using LSCF [13, 15]. Moreover, the LSCF utilizes an iterative optimization process to determine BFSs from a large number of BGSs, particularly when the fiber is quite long. Each BGS also contain several hundreds of measurement points. As a result, the estimation of BFSs using LSCF becomes time-consuming [12].

It is necessary to achieve low UTM as well as to maintain ESR for precise temperature measurement with BOTDA sensors [9, 10]. The UTM relies on the SNR of the acquired experimental BGSs and ESR is linked to the width of pump-pulses [15, 16]. Short pump pulses are necessary to achieve better spatial resolution with BOTDA sensors. However, such pulses lead to very short pump-probe interaction times and provide BGSs with low SNR [14]. Consequently, there is a trade-off between UTM and ESR. At a fixed ESR, the averaging operation on BOTDA-traces is a frequently-used technique used to enhance the SNR of BGSs obtained from BOTDA sensors [15]. This technique involves averaging multiple sweeps of measurements taken at the same point

along the fiber. While trace averaging of a large number of traces is a useful technique to get better SNR, it can significantly slow down the measurement process. To strike a balance between UTM and acquisition time, we can alternately use averaging operation on a small number of traces during the experiment, and then apply a suitable noise reduction filters to denoise them. Different denoising algorithms are used for such purpose, some of which includes anisotropic diffusion filter [17], wavelet transform [18, 19], cross-correlation [12, 20] and non-local means filter [21 - 23]. The use of these noise reduction filters can enhance SNR but the selection of improper filters can have a detrimental effect on ESR [19]. Thus, it is crucial to analyze the impact of these denoising algorithms on experimental spatial resolution (ESR) and signal processing speed (SPS) which have been largely overlooked in the literatures.

In this study, we have accurately extracted temperature distributions over a 38.2 km SMF. For such accurate temperature extraction, we have first explored the impact of using six different noise reduction filters for improving SNR of BGSs. In addition, we have analyzed the benefits of using these filters in terms of UTM, ESR and SPS.

2. Experimental Setup and Acquisition of BGSs

As shown in Fig.1, a conventional BOTDA sensor [7, 12] uses a continuous-wave (CW) laser source emitting 1550 nm light that passes through upper and lower branches after being divided by the coupler. The PC1 and PC2 regulate the SOP of light waves passing through two branches. Here, PC and SOP stand for polarization controller and state-of-polarization, respectively.

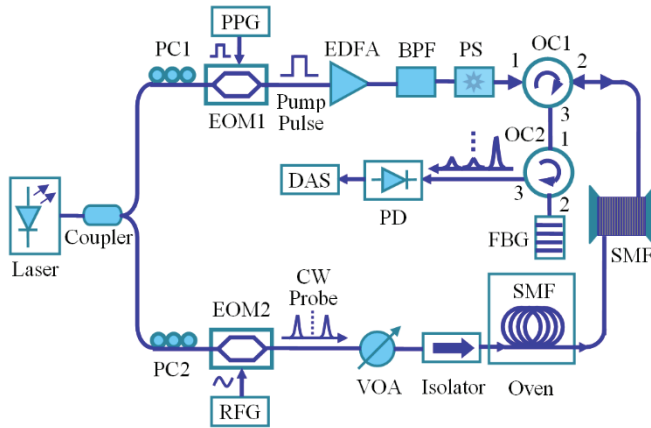


Fig. 1. A conventional BOTDA sensor.

The upper branch in Fig. 1 uses a pulse pattern generator (PPG) to control an electro-optic modulator (EOM1), which modifies the CW wave to generate pump pulses. An erbium-doped fiber amplifier (EDFA) is then employed to amplify the pump pulses. The amplified spontaneous emission (ASE)

noise produced during amplification process is reduced by using a band pass filter (BPF), while a polarization scrambler (PS) diminishes the polarization-induced fading of Brillouin gain. The upper branch also includes an optical circulator (OC1) that direct light from ports '1' and '2', enabling pump-pulses to launch from the upper branch to the near end of the SMF. The lower branch uses the radio-frequency generator (RFG) to create probe wave with double sideband suppressed carrier (DSB-SC) via EOM2. The power of DSB-SC probe wave is controlled by a variable optical attenuator (VOA), which directs such wave through an optical isolator, preventing reverse light propagation through the SMF.

The setup, depicted in Fig. 1, involves the reverse propagation of pump and probe waves within the SMF, delivering power from the pump wave to intensify the probe wave. The setup uses OC2 to transmit the probe wave to a FBG filter, thereby selecting the intended sideband in the lower frequency region. Such sideband is detected by the photo-detector (PD). The data acquisition system (DAS) collects BOTDA-traces and assembles them as BGSs, which are first denoised and then processed for extracting temperature distribution along the SMF.

3. Principles of Noise Reduction Filters

In this study, we have treated noisy experimental BGSs acquired from the BOTDA sensor as an image and denoised such image using various noise reduction filters.

3.1 Bilateral Filter (BF)

The BF is a local, nonlinear and non-iterative filtering technique to reduce noise from images while preserving edges. This filter utilizes geometric closeness of the neighboring pixels and replaces the value of a pixel by the weighted average of its neighboring pixels [24, 25]. The BF filtered image value at a pixel location m of an original image value I_m is defined [24] by

$$I_m^{BF} = \frac{1}{F_m} \sum_{n \in S} G_{\sigma_s}(\|m - n\|) G_{\sigma_r}(|I_m - I_n|) I_n \quad (1)$$

where, S is a spatial neighborhood of m , I_n is the image value at pixel position n and $\|m - n\|$ is the Euclidean distance between m and n . The BF filter given by Eq. (1) uses the geometric closeness function $G_{\sigma_s}(\cdot)$, the gray level similarity function $G_{\sigma_r}(\cdot)$ and the normalization factor F_m as given by Eq. (2), Eq. (3) and Eq. (4), respectively [25].

$$G_{\sigma_s}(\|m - n\|) = \exp(-\|m - n\|^2 / 2\sigma_s^2) \quad (2)$$

$$G_{\sigma_r}(|I_m - I_n|) = \exp(-|I_m - I_n|^2 / 2\sigma_r^2) \quad (3)$$

$$F_m = \sum_{n \in S} G_{\sigma_s} (\|m - n\|) G_{\sigma_r} (|I_m - I_n|) \quad (4)$$

The parameters σ_s and σ_r in Eq. (2) and Eq. (3) determines the amount of filtering on the image and F_m given by Eq. (4) ensures that pixel weights sum to 1 [24].

3.2 Guided Filter (GF)

The GF proposed by K. He et al. [26] is a local, linear and fast edge-preserving filter that provides the denoised image based on a guided image considering local spatial neighborhood statistics [26, 27]. The guided image can be the image itself [27]. There is a linear relationship between input image I_m , the guided image G_m and the filtered image in a local window ω_c as given by

$$I_m^{GF} = a_c G_m + b_c, \quad \forall m \in \omega_c \quad (5)$$

where, a_c and b_c are constant coefficients within ω_c . The noise components N_c can be given by

$$I_m - I_m^{GF} = N_c \quad (6)$$

The difference given by Eq. (6) in the window ω_c is minimized by minimizing the function $E(a_c, b_c)$ as given by

$$E(a_c, b_c) = \sum_{m \in \omega_c} \left[(a_c G_m + b_c - I_m)^2 + \lambda a_c^2 \right] \quad (7)$$

where, λ is a regularization parameter. The Eq. (7) can be solved using linear regression [26] to obtain

$$a_c = \frac{\left(\frac{1}{|\omega|} \sum_{m \in \omega_c} G_m I_m \right) - \mu_c \bar{I}_c}{\sigma_c^2 + \lambda}, \text{ and} \quad (8)$$

$$b_c = \bar{I}_c - a_c \mu_c \quad (9)$$

Where $|\omega|$, μ_c and σ_c^2 are total number, mean and variance of pixels, respectively in ω_c , while \bar{I}_c is the mean of m in ω_c . The output I_m^{GF} can now be obtained using Eq. (5) as given by

$$I_m^{GF} = \frac{1}{|\omega|} \sum_{m \in \omega_c} (a_c I_m + b_c) \quad (10)$$

where, I_m is the value of noisy image and I_m^{GF} is the guided filtered image values at pixel location m .

3.3 Adaptive Wiener Filter (AWF)

For reducing noise from experimental BGSs using AWF, BGSs along the SMF are grouped as a 2D image $B(m, n)$. The denoising process utilizes neighborhood pixels to determine the local image mean and variance [28, 29]. The AWF uses its M -by- N neighborhood pixels to determine mean (\bar{a}) for local image as given by

$$\bar{a} = \frac{1}{MN} \sum_{m, n \in \beta} B(m, n) \quad (11)$$

where, β represents $M \times N$ local neighborhood of current pixel in $B(m, n)$. The variance (σ^2) for the local image is given by

$$\sigma^2 = \frac{1}{MN} \sum_{m, n \in \beta} E^2(m, n) - \bar{a}^2. \quad (12)$$

The AWF filtered value of each pixel in $B(m, n)$ is next approximated to be [28]

$$D^{AWF}(m, n) = \bar{a} + \frac{\sigma^2 - \sigma_n^2}{\sigma^2} [B(m, n) - \bar{a}] \quad (13)$$

In Eq. (13), σ_n^2 represents the variance of noise. It is remarkable in Eq. (13) that the noise reduction using AWF is influenced by σ^2 , with smaller reductions for larger values and larger reductions for smaller ones. As a result, AWF works adaptively to maintain high-frequency components of $B(m, n)$ and thus preserves edges.

3.4 Non-Local Means Filter (NLMF)

The NLMF effectively reduces noise in an image by using weighted average of image pixels' intensities to estimate a pixel's intensity, calculated based on pixel resemblance and surrounding pixels' similarity [30, 31]. The weighted average computation involves a search window S_m that contains a given pixel number adjacent to the pixel m . In non-local means filter, the value of denoised pixel $D(m)$ of a noisy pixel $B(m)$ is estimated by [31]

$$D^{NLM}(m) = \sum_{n \in S_m} w(m, n) B(n) \quad (14)$$

where S_m is the search window of size $S \times S$ centering pixel m . The resemblance between pixels m and n is assessed using a declining function [32] given by

$$t(m, n) = \left\| B(N_m) - B(N_n) \right\|_{2, \sigma}^2 \quad (15)$$

where, σ represents the standard deviation of the Gaussian kernel. In Eq. (15), the intensity of pixels in a $C \times C$ comparison window centered on pixels m and n within the search window S_m is denoted by $B(N_m)$ and $B(N_n)$. The weight $w(m, n)$ in Eq. (14) are then calculated [31, 32] by

$$w(m, n) = \frac{1}{h(m)} e^{-\frac{t(m, n)}{d^2}}. \quad (16)$$

where, d is the standard deviation of noise estimated from the noisy Brillouin gain spectra. It is used to adjust the degree of smoothing in non-local means filtering and the normalization

constant $h(m)$ in Eq. (16) ensures that $0 \leq w(m,n) \leq 1$ and $\sum_n w(m,n) = 1$.

3.5 Average Filter (AF)

The AF is a linear filter which employs mean values for replacing the pixel values of the original image. This filter uses a rectangular window made up of a number of pixels from the neighbor centering the current pixel (m, n) . The filtered value of a pixel using AF is determined by [33]

$$D^{AF}(m,n) = \frac{1}{W_p} \sum_{B \in W} B(m,n) \quad (17)$$

where, W is a local window that consists of a total number of W_p pixels including the current pixel.

3.6 Disc Filter (DF)

The DF is also known as circular averaging filter in which the averaging operation on the pixels is calculated over a circular window surrounding a pixel.

4. Principle of Least-Squares Curve Fitting (LSCF)

For the extraction of temperature distributions throughout the SMF, LSCF [7, 10] is exploited to find BFSs of experimental and denoised BGSs separately. In such fitting, each BGS along the SMF are fitted with the Lorentzian function given by

$$g(\nu) = \frac{g_p}{1 + 4 \left[(\nu - \nu_p) / \Delta \nu_p \right]^2} \quad (18)$$

where g_p , ν_p and $\Delta \nu_p$ are respectively the peak gain, frequency at g_p (BFS) and linewidth of a BGS. The comprehensive explanation of LSCF is available in Ref [7, 11].

After completing LSCF process, the fitted BFSs along the SMF are determined. Then, the fitted BFSs are transformed to temperature using the linear relation between them with ~ 0.975 MHz/°C slope and 10.834 GHz intercept [7]. In this study, the SNR of experimental as well as denoised BGS along the SMF are determined by [7, 17]

$$SNR(dB) = 10 \log_{10} \left(\frac{g_p^2}{\sigma_r^2} \right) \quad (19)$$

where σ_r denotes the standard deviation of residuals which is the difference between the experimental BGS and the fitted BGS. A typical experimental BGS, its fitted BGS and residuals are depicted in Fig. 2.

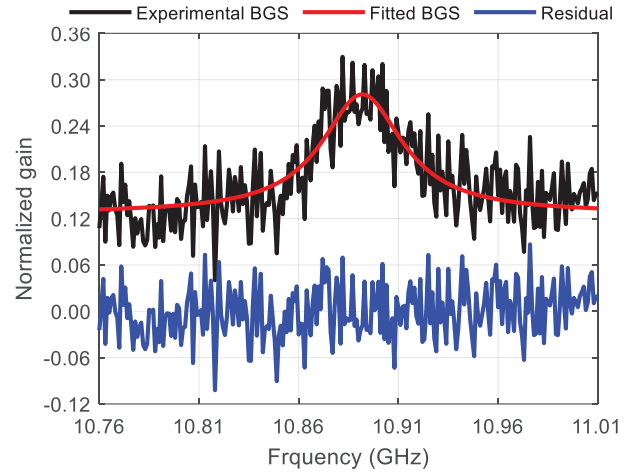


Fig. 2. A typical experimental BGS, its fitted BGS and residuals.

5. Experimental Results and Discussion

The experiment involved placing a 38.2 km SMF in the BOTDA sensor setup depicted in Fig. 1. To evaluate the performance of the temperature sensor, ~ 0.59 km from the end of the SMF is heated in an oven while the remaining SMF (i.e., ~ 37.61 km) is retained at room temperature of ~ 25 °C outside the oven. The oven temperature is set at 60 °C. The pump-pulses width is tuned to 20 ns for fixing 2 m ESR of the sensor. The DAS in Fig. 1 acquires BOTDA-traces along the SMF with PD output sampled at 125 Mega-symbols/second that fixed the distance between two consecutive samples in the traces to be 0.4 m. To obtain a single BOTDA-trace along the 38.2 km SMF at a particular frequency, the averaging of 100 traces is adopted. The BGSs along the SMF are formed by combining 251 traces collected at frequencies spanning from 10.76 GHz to 11.01 GHz adopting uniform frequency step of 1 MHz. These BGSs are shown in Fig. 3.

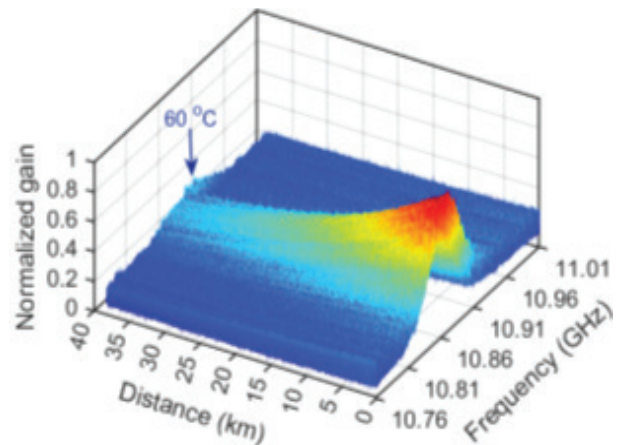
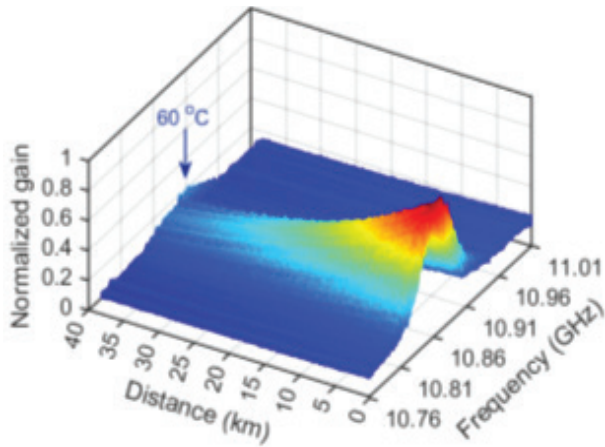


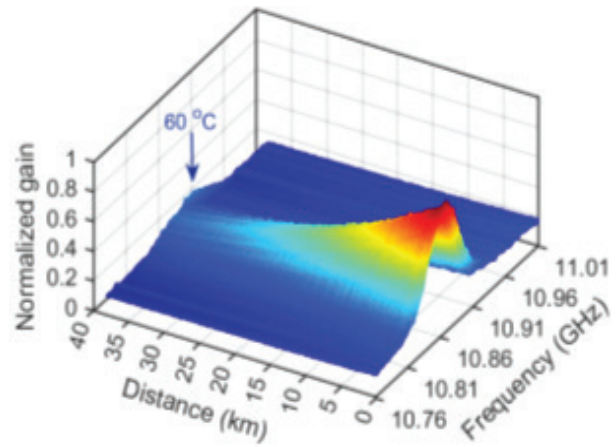
Fig. 3. Distribution of experimental BGSs over 38.2 km SMF with last ~ 0.59 km fiber at 60 °C.

The BGSs in Fig. 3 show that the normalized gains of BGSs at the beginning of the SMF is maximum, decreasing gradually with distance due to the attenuation of signals propagating through the SMF. The most significant observation in Fig. 3 that the BFSs (central frequencies) of BGSs along the last part (~0.59 km) of the SMF have been shifted to higher frequency due to applying 60 °C inside the oven compared to the part of the SMF put outside the oven at ~25 °C. The BGSs in Fig. 3 also show a significant increase

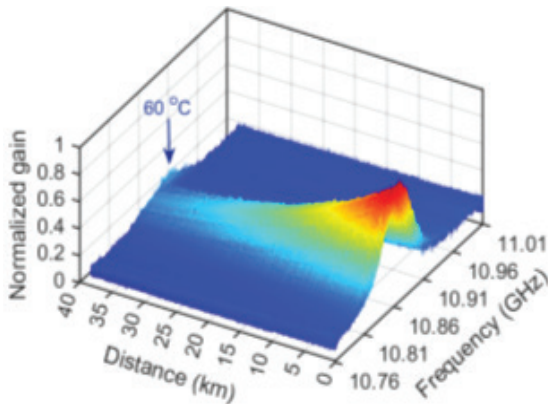
in noise level along the SMF due to noise accumulation. The noise levels in the experimental BGSs along the SMF shown in Fig. 3 are first reduced separately by applying different noise reduction filters as described in section 3. To explore the effectiveness, six different noise reduction filters (i.e., BF, GF, AWF, NLMF, AF, and DF) are adopted in this study. The denoised BGSs obtained after applying such noise reduction filters are exhibited in Fig. 4 (a)–(f).



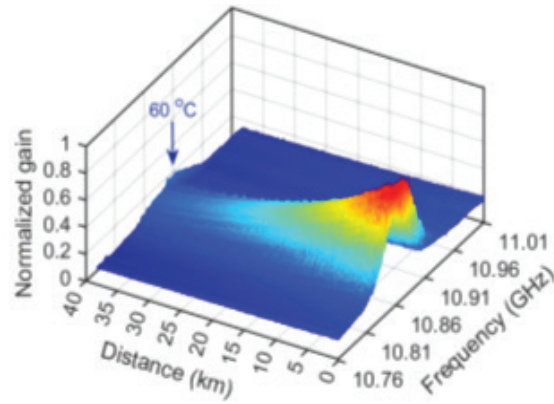
(a) BGSs denoised by bilateral filter (BF)



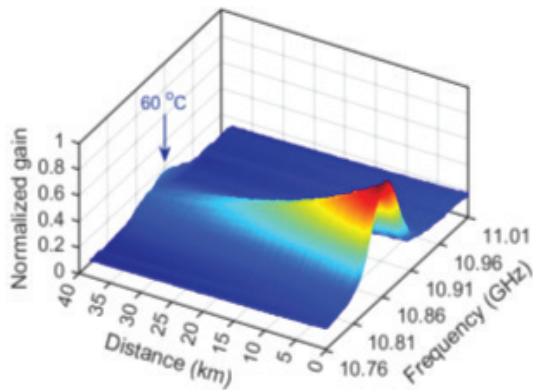
(b) BGSs denoised by guided filter (GF)



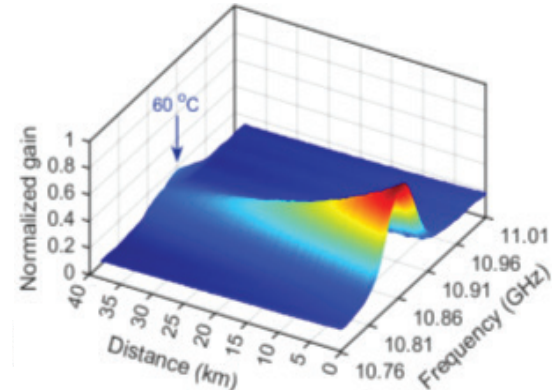
(c) BGSs denoised by adaptive Wiener filter (AWF)



(d) BGSs denoised by non-local means filter (NLMF)



(e) BGSs denoised by average filter (AF)



(f) BGSs denoised by disc filter (DF)

Fig. 4. Distributions of denoised BGSs over 38.2 km SMF with last ~0.59 km fiber at 60 °C.

It is noticed that the BGSs in Fig. 4 are much smoother than that in Fig. 3. This means that the noise levels in denoised BGSs are much smaller than that in noisy experimental BGSs. The reduced noise in the denoised BGSs is actually due to the fact that the noise reduction filters help to reduce noise from BOTDA traces that collectively construct BGSs along the SMF. To observe the effects of noise reduction filters on BOTDA traces, one of the traces along the SMF at 10.854 GHz and its denoised traces obtained after applying six different noise reduction filters are shown in Fig. 5.

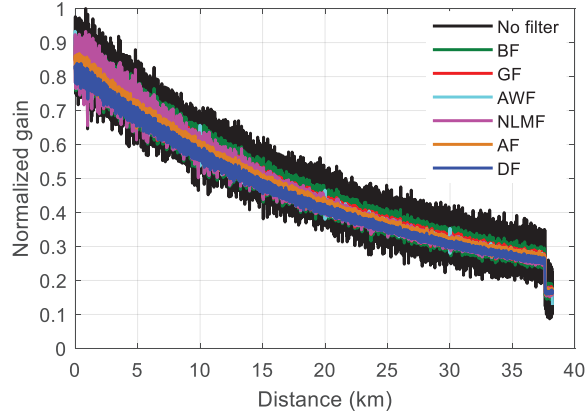


Fig. 5. Experimental and denoised traces over 38.2 km SMF.

The comparison of traces in Fig. 5 manifests that the fluctuations of normalized gain of denoised traces obtained after applying noise reduction filters are much smaller than that of unfiltered noisy trace. As a result, the levels of noise in filtered BGSs in Fig. 4 are smaller than that of noisy BGSs in Fig. 3. Consequently, the SNRs of denoised BGSs are much improved compared to noisy experimental BGSs. To quantify such SNR improvement, we have also determined the SNR of each BGS along the SMF. For this, each noisy or denoised BGS along the SMF is curve-fitted with Lorentzian function defined by Eq. (18). The SNR of each BGS along the SMF is then calculated by Eq. (19). The distributions of such SNR along the 38.2 km SMF are shown in Fig. 6.

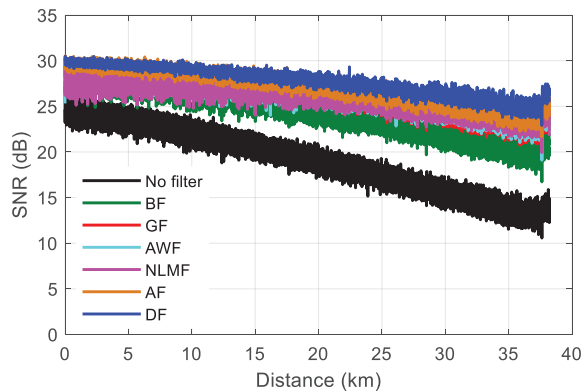


Fig. 6. SNRs of experimental and denoised BGSs over 38.2 km SMF.

The results presented in Fig. 4, Fig. 5 and Fig. 6 signify that the noise reduction filters help to reduce the levels of noise of experimental BGSs, i.e., SNR is improved. The temperature distributions extracted from such denoised BGSs also provides lower uncertainty in temperature measurement (UTM). To verify this, the temperature distributions have then been extracted from both experimental and denoised BGSs as shown in Fig. 3 and Fig. 4, respectively by applying the process of temperature extraction described in section 4. The results in Fig. 7 display temperature distributions from experimental and denoised BGSs for comparison purposes.

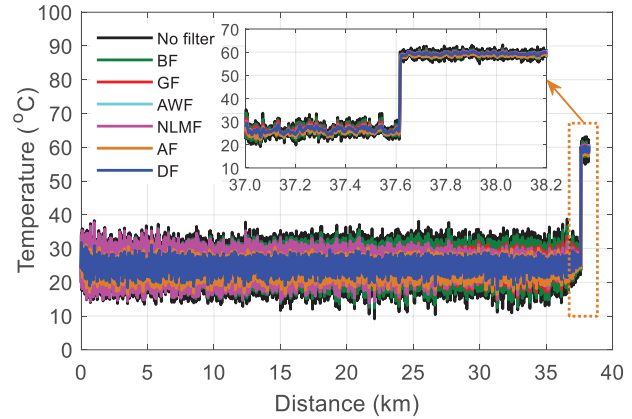


Fig. 7. Temperature distributions over 38.2 km SMF with last ~0.59 km heated at 60 °C. Inset: Temperature distributions over last 1.2 km.

It is clear in Fig. 7 that the fluctuations in extracted temperature from denoised BGSs obtained after applying BF, GF, AWF, NLMF, AF and DF are much lower than that extracted from noisy experimental BGSs without applying any noise reduction filter. Such lower fluctuation in temperature distributions manifests that the use of noise reduction filters can provide lower UTM.

The distributions of SNR along the SMF in Fig. 6 clearly exhibit that noise reduction filters notably improve the SNR of experimental noisy BGSs, reducing fluctuations in extracted temperature distributions as can be seen in Fig. 7. The working principle of noise reduction filters are based on smoothing operation. Such smoothing operation using a filter may adversely affect on the original BGSs, especially where there are shifts of BGSs to higher frequency due to applying higher temperature. As a result, the ESR of BOTDA sensors may deteriorate from the experimental value of 2 m. To verify such effect on the ESR of the sensor, the extracted temperature distributions after applying six different noise reduction filters along the segment of SMF (i.e., 37.612 km to 37.619 km) at which temperature distributions change sharply from ~25 °C to 60 °C are shown in Fig. 8. The temperature distribution extracted from the experimental

BGSs over the same segment of SMF is also drawn in the same Fig. 8 for the purpose of comparison.

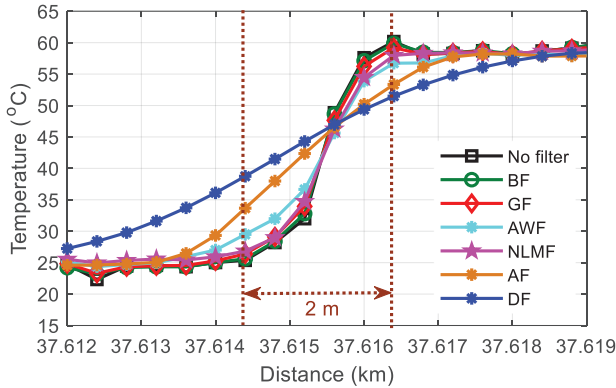


Fig. 8. Transitions of temperature from room temperature (~ 25 °C) to 60 °C to show experimental spatial resolution (ESR).

During the acquisition of BGSs from the BOTDA setup shown in Fig. 1, the pump-pulses having width of 20 ns were adopted that corresponds to the ESR of 2 m. The distribution of temperature for the noisy experimental BGSs with no filter in Fig. 8 also verifies such ESR. The temperature transitions in Fig. 8 show that AWF can nearly preserve such ESR but that of AF and DF fails to preserve ESR of 2 m. However, three noise reduction filters (i.e., BF, GF and NLMF) can strictly maintain 2 m ESR as can be observed in Fig. 8. The demonstration of spatial resolution in Fig. 8 suggest that BF, GF and NLMF can be considered as the effective noise reduction filters for denoising BGSs obtained from BOTDA sensors if the preservation of ESR is considered only.

This study quantitatively assessed the efficacy of six distinct noise reduction filters in terms of SNR, UTM, ESR and SPS. For such quantitative analysis, we have considered a total of 1251 BGSs each spaced at a distance of 0.4 m along the last 0.5 km SMF where the SNRs are the worst. For the analysis of SNR improvement, each experimental BGS along the SMF are fitted by applying LSCF. The SNR of each experimental BGS is then quantified by Eq. (19). Then, the SNRs calculated for all of the 1251 BGSs along the last 0.5 km SMF are all averaged to find the experimental SNR of the BGSs. The process is repeated to find the SNR of denoised BGSs after employing each of the six different noise reduction filters separately. For the quantitative analysis of UTM, we have extracted temperature distributions from the noisy BGSs without filtering operation and that from the filtered BGSs after utilizing each of the six filters. The UTM is calculated as the standard deviation of extracted temperatures over the last 0.5 km SMF. For analyzing the relative runtime, we have recorded the runtime

elapsed for extracting temperature distributions from 3001 BGSs along the last 1.2 km SMF. For the experimental BGSs, the runtime is calculated to be the time elapsed to extract temperature from the experimental BGSs directly without applying any filter. However, the runtime of extracting temperature from the denoised BGSs accounts the time elapsed for denoising noisy BGSs with filter plus the time elapsed for applying LSCF to extract temperature along the SMF. Finally, the signal processing speed (SPS) is computed to be the ratio of runtime elapsed for extracting temperature from noisy experimental BGSs to that from noisy or denoised BGSs. Thus, higher SPS represents faster temperature extraction compared to extracting temperature from noisy BGSs. The performances of different noise reduction filters along with the status of ESR preservation shown in Fig. 8 for noisy and denoised BGSs are listed in Table 1.

Table 1. Performances of different noise reduction filters

Filter	SNR (dB)	UTM (°C)	ESR (~ 2 m)	SPS
---	13.77	1.198	Preserved	1.000
BF	15.95	1.003	Preserved	1.071
GF	17.73	0.836	Preserved	1.110
AWF	24.14	0.495	Nearly Preserved	1.080
NLMF	23.99	0.492	Preserved	1.062
AF	24.91	0.471	Not preserved	1.091
DF	26.38	0.393	Not preserved	1.122

As indicated in Table. 1, the SNR of denoised BGSs obtained through each of the six different noise reduction filters improves significantly in contrary to that of the noisy BGSs. Thus, the UTM also reduces appreciably. Although the SNR and UTM provided by AWF, NLMF, AF and DF are much better as compared to that obtained for noisy BGSs without filter, only NLMF can preserve the ESR, which is 2 m in this study. On the other hand, BF and GF can preserve the ESR but the SNR and UTM provided by these two filters are much lower and higher, respectively. Among six different noise reduction filters, the results presented in Table. 1 manifest that only NLMF can provide reasonably higher SNR and lower UTM and can preserve ESR of 2 m. For using NLMF, the SNR can be improved by 10.22 dB from 13.77 dB (for noisy BGSs) to 23.99 dB. For such improvement of SNR, the UTM can be improved from 1.198 °C to 0.492 °C (i.e., 58.93%). Moreover, the SPS for extracting temperature distribution after applying NLMF is 1.062, which is 6.2% higher than that without applying any filtering operation on experimental BGSs. Although the use of NLMF before

applying LSCF to extract temperature distribution takes additional runtime, the SNR of denoised BGSs becomes much higher as compared to noisy BGSs as shown in Table. 1. As a result, the iterative procedure in LSCF takes shorter runtime for temperature extraction from denoised BGSs having improved SNR. Thus, the total runtime of using NLMF plus LSCF is relatively shorter as compared to that of using LSCF directly on the noisy experimental BGSs. The SNR, UTM, ESR and SPS listed in Table. 1 reveal that the performance of NLMF is the best among six noise reduction filters applied in this study.

6. Conclusions

In this study, the noise reduction filters and LSCF based distributed temperature extraction from BGSs along a 38.2 km SMF have been demonstrated and analyzed. Six different noise reduction filters have been adopted in such demonstration and their performances have been compared in terms of SNR, UTM, ESR and SPS. The results show that AF and DF provides highest SNR and lowest UTM but completely fail to preserve the ESR. The AWF performs well in terms of SNR and UTM but it cannot preserve ESR perfectly. However, three other noise reduction filters (i.e., BF, GF and NLMF) can preserve ESR perfectly but the SNR (23.99 dB) and the UTM (0.492 °C) performances of NLMF are the best among these three filters. The SPS for using NLMF and LSCF based temperature extraction is also a little bit faster than that for using LSCF directly without applying any filter. Thus, the use of NLMF effectively reduces noises from BGSs and preserves ESR perfectly, making BOTDA sensors more viable for high-accuracy applications. The future study will research on the use of NLMF and machine learning for precise, ESR-preserved and ultra-fast BOTDA sensors.

Acknowledgement

The authors acknowledge financial support from the University Grants Commission (UGC) of Bangladesh under UGC Research grant (2022-23) for the University of Dhaka and express gratitude to the Photonics Research Institute at Hong Kong Polytechnic University, Hong Kong SAR for the experiment facility.

References

1. D. Iida, N. Honda, and H. Oshida, 2020, "Advances in distributed vibration sensing for optical communication fiber state visualization," *Opt. Fiber Technol.* 102263, 57, pp. 1-9.
2. A. Coscetta, A. Minardo, and L. Zeni, 2020, "Distributed Dynamic Strain Sensing Based on Brillouin Scattering in Optical Fibers," *Sensors* 5629, 20(19), pp. 1-23.
3. Y. Wang, H. Yao, J. Wang and X. Xin, 2022, "Distributed Optical Fiber Sensing System for Large Infrastructure Temperature Monitoring," *IEEE Internet of Things Journal*, 9(5), pp. 3333-3345.
4. T. Wu, G. Liu, S. Fu and F. Xing, 2020, "Recent Progress of Fiber-Optic Sensors for the Structural Health Monitoring of Civil Infrastructure," *Sensors*, 20(16), pp. 4517.
5. D. Iida, N. Honda, and H. Oshida, 2020, "Advances in distributed vibration sensing for optical communication fiber state visualization," *Opt. Fiber Technol.* 102263, 57, pp. 1-9.
6. M. A. M. ohnson, S. K. Phang, W. R. Wong, W. J. Chew, H. K. Mun, Y. Hoon, 2023, "Distributed fiber optic sensing in landslide monitoring – A comparative review" *J. Engg. Sci Technol*, 18(1), pp. 406-423.
7. A. K. Azad, F. N. Khan, W. H. Alarashi, N. Guo, A. P. T. Lau and C. Lu, 2017, "Temperature extraction in Brillouin optical time-domain analysis sensors using principal component analysis based pattern recognition," *Opt. Express*, 25(14), pp. 16534-16549.
8. P. Xu, Y. Dong, D. Zhou, C. Fu, J. Zhang, H. Zhang, Z. Lu, L. Chen and X. Bao, 2016, "1200°C high-temperature distributed optical fiber sensing using Brillouin optical time domain analysis," *Appl. Opt.*, 55(21), pp. 5471-5478.
9. S. Wang, Z. Yang, S. Zaslowski, and L. Thévenaz, 2020, "Short spatial resolution retrieval from a long pulse Brillouin optical time-domain analysis trace," *Opt. Lett.*, 45(15), pp. 4152-4155.
10. X. Angulo-Vinuesa, S. Martin-Lopez, P. Corredera, and M. Gonz'alez-Herr'aez, 2012, "Raman-assisted Brillouin optical time-domain analysis with sub-meter resolution over 100 km," *Opt. Express*, 20(11), pp. 12147-12154.
11. A. Motil, A. Bergman, and M. Tur, 2016, "State of the art of Brillouin fiber-optic distributed sensing," *Opt. & Laser Technol.*, 78(A), pp. 81-103.
12. A. K. Azad, L. Wang, N. Guo, H. Y. Tam and C. Lu, 2016, "Signal processing using artificial neural network for BOTDA sensor system," *Opt. Express*, 24(6), pp. 6769-6782.
13. S. Wang, Z. Yang, M. A. Soto and L. Thévenaz, 2020, "Study on the signal-to-noise ratio of Brillouin optical-time domain analyzers," *Opt. Express*, 28(14), pp. 19864-19876.
14. J. E. Kadum, C. Feng, T. Schneider, 2020, "Characterization of the Noise Induced by Stimulated Brillouin Scattering in Distributed Sensing," *Sensors*, 20(15), pp. 1-15.
15. M. A. Farahani, M. T. V. Wylie, E. Castillo-Guerra, and F. G. Colpitts, 2012, "Reduction in the number of averages required in BOTDA sensors using wavelet denoising techniques," *J. Lightwave Technol.* 30(8), pp. 1134-1142.
16. M. A. Soto, and L. Thévenaz, 2013, "Modeling and evaluating the performance of Brillouin distributed optical fiber sensors," *Opt. Express*, 21(25), pp. 31347-31366.
17. K. Luo, B. Wang, N. Guo, K. Yu, C. Yu, and C. Lu, 2020 "Enhanced SNR by Anisotropic Diffusion for Brillouin Distributed Optical Fiber Sensors," *J. Lightwave Technol.* 38(20), pp. 5844-5852.
18. M. A. Soto, J. A. Ramírez, and L. Thévenaz, 2016, "Intensifying the response of distributed optical fibre sensors using 2D and 3D image restoration," *Nat. Commun.* 10870, 7, pp. 1-11.

19. A. K. Azad, 2020, "Analysis of 2D Discrete Wavelet Transform Based Signal Denoising Technique in Brillouin Optical Time Domain Analysis Sensors," *The Dhaka University JASE*, 5(1&2), pp. 1-8.
20. M. A. Farahani, E. Castillo-Guerra, and B. G. Colpitts, 2013, "A Detailed Evaluation of the Correlation-Based Method Used for Estimation of the Brillouin frequency shift in BOTDA sensors," *IEEE Sensors J.*, 13(12), pp. 4589-4598.
21. X. Qian, X. Jia, Z. Wang, B. Zhang, N. Xue, W. Sun, Q. He and H. Wu, 2017, "Noise level estimation of BOTDA for optimal non-local means denoising," *Appl. Opt.*, 56(16), pp. 4727-4734.
22. M. A. Soto, J. A. Ramírez, and L. Thévenaz, 2018, "Optimizing Image Denoising for Long-Range Brillouin Distributed Fiber Sensing," *J. Lightwave Technol.* 36(4), pp. 1168–1177.
23. A. K. Azad, 2022, "Robust Signal Denoising Techniques for Highly Accurate and Spatial Resolution Preserved Brillouin Optical Time Domain Analysis Sensors," *The Dhaka University JASE*, 7(2), pp. 31-38.
24. S. Paris, P. Kornprobst, J. Tumblin and F. Durand, 2008, "Bilateral Filtering: Theory and Applications," *Foundations and Trends in Computer Graphics and Vision*, 4(1), pp. 1-73.
25. B. K. S. Kumar, 2013, "Image denoising based on gaussian/bilateral filter and its method noise thresholding" *Signal, Image and Video Processing*, 7(6), pp. 1159–1172.
26. K. He, J. Sun, X. Tang, 2010, "Guided Image Filtering. Computer Vision – ECCV 2010, Lecture Notes in Computer Science, 6311(1) Springer, Berlin, Heidelberg, pp. 1-14.
27. S. Zhu and Z. Yu, 2020, "Self-Guided Filter for Image Denoising" *IET Image Processing*, 14(11), pp. 2561-2566.
28. S. K. Jadwa, 2018, "Wiener Filter based Medical Image Denoising," *Int. J. Sci. & Engg. Applications*, 7(9), pp. 318-323.
29. F. Wu, W. Yang, L.Xiao, and J. Zhu, 2020, "Adaptive Wiener Filter and Natural Noise to Eliminate Adversarial Perturbation," *Electronics* 1634, 9(10), pp. 1-14.
30. D. Dhillon, D. Chouhan, Rajlaxmi, 2022, "Edge-preserving image denoising using noise-enhanced patch-based non-local means" *Multimedia Systems* 29, pp. 1025-1041.
31. B. K., S. Kumar, 2013, "Image denoising based on non-local means filter and its method noise thresholding," *Signal, Image and Video Processing*, 7(1), pp. 1211-1227
32. K. M. Prabusankarlal, R. Manavalan, and R. Sivaranjani, 2018, "An optimized non-local means filter using automated clustering based preclassification through gap statistics for speckle reduction in breast ultrasound images," *App. Computing and Informatics*, 14(1), pp. 48-54.
33. T. Li, J. Wang, and K. Yao, 2022, "Visibility enhancement of underwater images based on active polarized illumination and average filtering technology," *Alexandria Engineering Journal*, 61(1), pp.701-708.